

Grain Physics and Rosseland Mean Opacities

Jason W. Ferguson^{1,2}, Amanda Heffner-Wong^{1,3}, Jonathan J. Penley¹, Travis S. Barman⁴,
David R. Alexander^{1,5}

ABSTRACT

Tables of mean opacities are often used to compute the transfer of radiation in a variety of astrophysical simulations from stellar evolution models to protoplanetary disks. Often tables, such as Ferguson et al. (2005), are computed with a predetermined set of physical assumptions that may or may not be valid for a specific application. This paper explores the effects of several assumptions of grain physics on the Rosseland mean opacity in an oxygen rich environment. We find that changing the distribution of grain sizes, either the power-law exponent or the shape of the distribution, has a marginal effect on the total mean opacity. We also explore the difference in the mean opacity between solid homogenous grains and grains that are porous or conglomerations of several species. Changing the amount of grain opacity included in the mean by assuming a grain-to-gas ratio significantly affects the mean opacity, but in a predictable way.

Subject headings: dust, extinction — equation of state — methods: numerical — astronomical data bases: miscellaneous

1. Introduction

The opacity of gaseous environments is a topic of interest in many areas of astrophysics including stellar atmospheres, circumstellar and protoplanetary disks, and the interstellar medium. Often, at least in the case of stellar evolution calculations, opacity tables are

¹Department of Physics, Wichita State University, Wichita, KS 67260-0032; jason.ferguson@wichita.edu

²visiting Max-Planck-Institut für Astrophysik, Karl-Schwarzschild-Str. 1, 85748 Garching, Federal Republic of Germany

³now at Project Zero, Harvard Graduate School of Education, 124 Mount Auburn Street, 5th Floor, Cambridge, MA 02138; amanda_heffner-wong@pz.harvard.edu

⁴Lowell Observatory, 1400 W. Mars Hill Rd., Flagstaff, AZ 86001; barman@lowell.edu

⁵now at Idaho State University; alexdavi@isu.edu

needed at many temperature, density and chemical composition points. For high temperature opacities modellers often use either the OPAL opacities (Iglesias & Rogers (1991, 1993, 1996), Rogers & Iglesias (1992a, 1992b) and Rogers et al. (1996)) or the Opacity Project (Seaton et al. 1994, OP hereafter) tables. We have produced low temperature opacities at Wichita State University (Ferguson et al. 2005, F05 hereafter) since 1975. These tables differ from their higher temperature counterparts by including the effects of molecules and dust in the equation of state (EOS hereafter) and the opacity.

Typical opacity tables provided by our group include over 1600 temperature and density points with 155 chemical compositions needed for a complete set. Given the large number of input variables, atomic and molecular physics, grain parameters for grain physics, etc., it is not computationally possible to make a complete set of opacity tables for every astrophysically significant situation. Difficult decisions must be made as to how to choose important physical parameters. For example, in the opacity tables of F05 grains are assumed to have a size distribution like the one described in a classic model (Mathis et al. 1977, MRN hereafter) based upon grain sizes in the interstellar medium (ISM); however this choice may not be appropriate for different astrophysical environments. This paper discusses some of the choices made in F05 and how those choices affect the total Rosseland mean opacity.

The calculations discussed here are taken from the same code used to complete the opacity tables described in F05, which includes a summary of the equation of state and opacities. For consistency we begin with the total Rosseland mean opacity, which is defined as

$$\frac{1}{\kappa_R} \equiv \frac{\int_0^\infty \frac{1}{\kappa_\lambda} \frac{\partial B_\lambda}{\partial T} d\lambda}{\int_0^\infty \frac{\partial B_\lambda}{\partial T} d\lambda} \quad (1)$$

where κ_λ is the monochromatic opacity and $\partial B_\lambda/\partial T$ is the derivative of the Planck function with respect to temperature. The monochromatic opacity includes the effects of all contributors:

$$\kappa_\lambda = \kappa_{cont} + \kappa_{at} + \kappa_{mol} + \kappa_{gr} \quad (2)$$

and includes continuous, atomic, molecular and grain sources of opacity. Note that the Rosseland mean is a harmonic mean, one in which individual contributors cannot be added after the mean is taken. This is particularly true of the molecular opacities which may have a large number of individual lines or bands. If it is desired that an individual source of opacity be modified, it is usually the case that the whole integral must be recomputed. A

detailed description of these sources is given in F05. We focus in this paper on the details of the grain contribution to the monochromatic opacity.

The opacity due to a particular dust species can be computed from

$$\kappa_{gr} \rho = \pi \sum_i \int_a n_i(a) Q_{\text{ext}}(a, i, \lambda) a^2 da \quad (3)$$

where $n_i(a)$ is the number of dust particles (cm^{-3}) of species i of size a and $Q_{\text{ext}}(a, i, \lambda)$ is the total extinction (absorption plus scattering) efficiency of the particle. The size distribution $n_i(a)$ depends upon both the number abundance of species i and on the size distribution of the dust particles. Ordinarily in our opacity tables the size distribution is taken from MRN, the classic distribution of dust sizes in the ISM given by

$$n_i(a) = ka^q \quad (4)$$

where k is a normalization constant of the distribution and q is the exponent of the power law. In F05 the value of q is taken to be the classical MRN value of -3.5.

Additional work by many other groups have resulted in other “favored” size distributions, however none have fully superseded the work of MRN (Clayton et al. (2003)). Other distributions such as Kim et al. (1995, KHM hereafter) and Weingartner & Draine (2001, WD hereafter) use power-laws as their basis, but include transitions for large grains so that the distribution behaves smoothly. For carbon grains WD, using the work of Draine & Li (2001) and Li & Draine (2001) go a step further and include multiple distributions for different sizes of grains. While this is not an exhaustive list of grain size distributions used in the astrophysical community today, it is representative of the types of grain models available. Each of the distributions listed have been inserted into our code for comparison with the MRN distribution.

In Eq. 3, the grain extinction efficiency is computed with Mie theory and assumes that grains are solid. This may not be the case in all, or any, astrophysical environments. Many researchers argue that interstellar grains are likely to be porous or “fluffy” in nature (see for example Mathis & Whiffen (1989), Mathis (1996), Chiar & Tielens (2006)). Having grains which are part vacuum can significantly affect their opacity (see Wolff et al. (1994), Wolff et al. (1998) and Voshchinnikov et al. (2005)). However, in astrophysical grains the amount of porosity, generally defined as the volume fraction of vacuum, is not well constrained; Chiar & Tielens (2006) interpret observations to constrain the porosity of dust in the ISM to be in the 25% to 50% range whereas Mathis (1996) indicates that dust may be

up to 80% vacuum.

Related to the porosity of grains is whether or not grains are composed of aggregates or are homogeneous. It is likely that astrophysical grains are not homogeneous as is assumed in the opacity tables of F05, but rather are an aggregate of two, three or more different species. The effect of heterogeneous grains on the mean opacity using the utilities of Ossenkopf (1991) will be discussed below.

The opacity tables of F05 assume that gas and dust are in equilibrium, but this may not be the case in real environments due to dynamical effects such as winds or gravitational settling of grains. One simple way to mimic the effects of grains either settling or being blown out of an environment is by changing the grain-to-gas ratio by assuming certain percentages of grain material have been removed from the gas.

This work is an exploration of the effects of grain physics on the total Rosseland mean opacity of a gas at cool temperatures (below ~ 3200 K). Opacities calculated here are for solar abundances, from Grevesse & Noels (1993) scaled to $X=0.7$ and $Z=0.02$ (where X is the mass fraction of hydrogen and Z is the mass fraction of metals), for $2.70 \leq \log T \leq 3.30$ and constant $\log R = -3.0$ (see F05). The value of $\log R = -3.0$ best models the atmosphere of an AGB-type star and was arbitrarily chosen here as a convenient way to demonstrate grain physics effects. All comparisons are done in an oxygen rich chemistry and include only silicate grains, future work will emphasize carbon grains. We will discuss five important aspects of grains physics in the following sections: (1) the size distribution exponent (see Eq. 4), (2) the size distribution itself, (3) grain porosity, (4) aggregate grains, (5) and the relative grain-to-gas ratio.

2. Grain Physics

In gas at high temperature, above ~ 5000 K, neutral and ionized atoms (including lines) are the dominant opacity sources. As the temperature decreases, molecular effects become significant and begin to dominate the opacity (see F05). Below ~ 1600 K at $\log R = -3.0$ grains begin to appear in the equation of state and quickly become the strongest source of opacity. For purposes of illustration, a plot similar to one from F05 is given in Figure 1 with the regions of dominant opacity marked. The features below $\log T = 3.2$ are caused by various grain species appearing or disappearing from the equation of state. At $\log T = 3.2$, solid Al_2O_3 appears in the EOS and causes a sudden rise in total opacity as the temperature decreases. Silicate grains begin to appear at $\log T \sim 3.08$. The opacity has another bump at $\log T = 3.02$ as solid Fe appears and becomes the dominant source of opacity. At

temperatures below $\log T = 3.0$ iron and silicates are the predominate opacity sources (F05); no additional significant species appear or disappear and the mean opacity is fairly featureless as it gradually lessens as the temperature decreases.

The opacity tables computed in F05 assumed spherical, solid, homogeneous grains with sizes that obey the MRN size distribution and with absorption and scattering cross-sections that can be simulated with Mie theory. We further assume in F05 that the grains form in equilibrium with and remain with the gas they form in. We will relax a few of these assumptions in the following sections to explore how the Rosseland mean opacity is affected.

2.1. Size Distribution Exponent

Equation 4 is a normalized power law distribution. As the value of the exponent, q , is varied – as the power law steepens or flattens – the size distribution will vary. As q increases the function will become steeper, that is, there are more small grains than large grains. The distribution is normalized for each grain species so that the volume of grain material is constant for the different values of q . The normalizations and summations are performed in terms of $\log(a)$, where a is the grain size.

As an illustration we include a plot of the “guts” of Eq. 3 in Figure 2. The figure shows how $Q(a)n(a)a^2$ behaves for a single grain species (Al_2O_3) and a single wavelength ($1 \mu\text{m}$). As the exponent of the size distribution increases from -2.5 to -5.5 , the size distribution, $n(a)$, steepens, but $Q(a)n(a)a^2$ flattens out. This flattening is due to the combination of the a^2 factor and the extinction efficiency Q increasing with size (as the grains are smaller than the Rayleigh limit) for the species shown.

What happens to the mean opacity if the value of the power law exponent, q , is varied from -2.5 to -5.5 ? Figure 3 shows that the mean opacity in the dust region ($\log T < 3.2$) increases as the power law flattens out. Considering Fig. 2 this result is not surprising. As the grain size distribution, q , flattens out the extinction efficiency, which is a function of grain size but not distribution, rises for larger grains. Thus a flatter grain size distribution contains more large grains and those larger grains contribute more to the total opacity.

The overall result for the mean opacity is that a flatter grain size distribution results in more opacity by as much as a factor of three when the power law exponent changes from -4.5 to -2.5 . It is easy to see the difference changing the exponent, q , to the mean opacity with the lower panel of Fig. 3. In the lower panel the logarithm of the ratio of the mean opacity computed with a certain q value compared with the baseline value of -3.5 is shown. This type of plot easily allows for the change in the mean opacity to be seen.

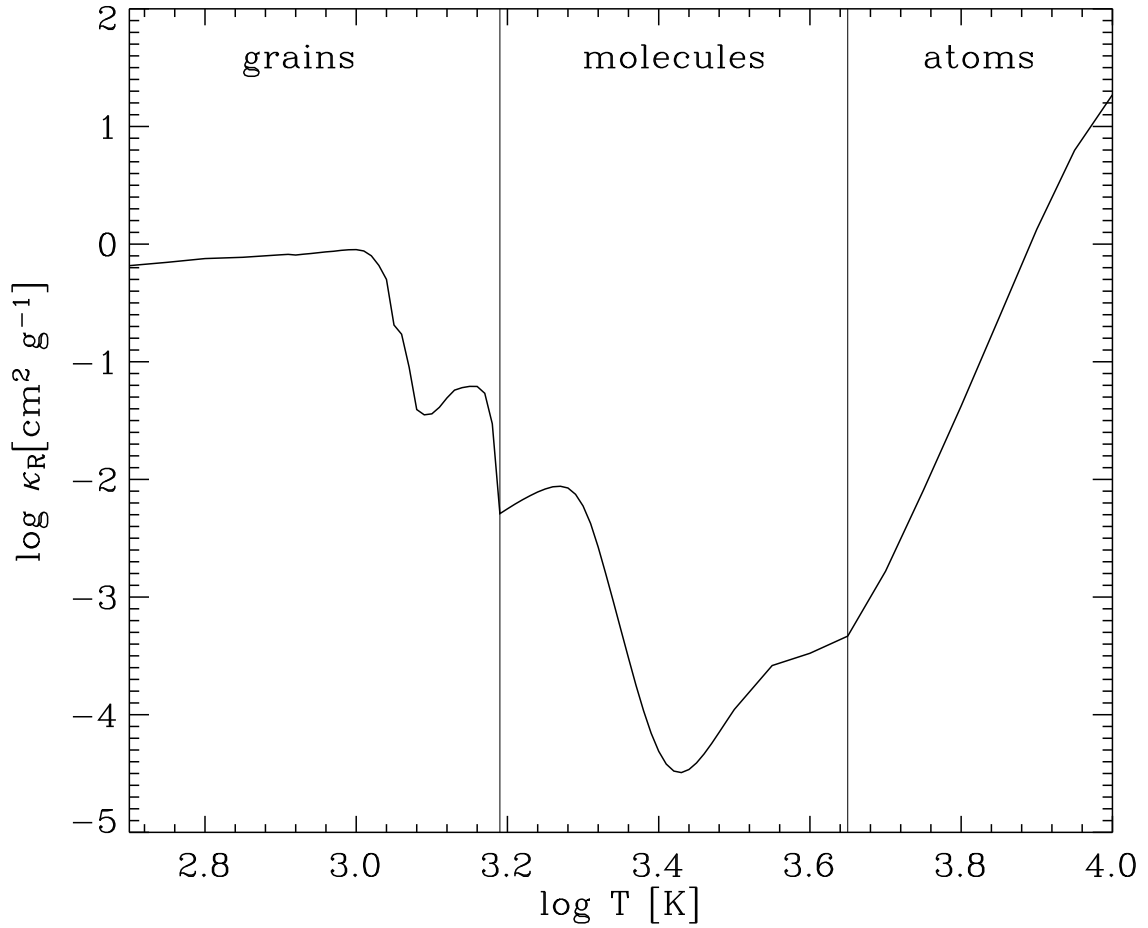


Fig. 1.— Logarithm of the total Rosseland mean opacity as a function of temperature for solar abundances and $\log R = -3.0$. Regions where different components dominate the opacity are indicated. Low temperature features are discussed in the text.

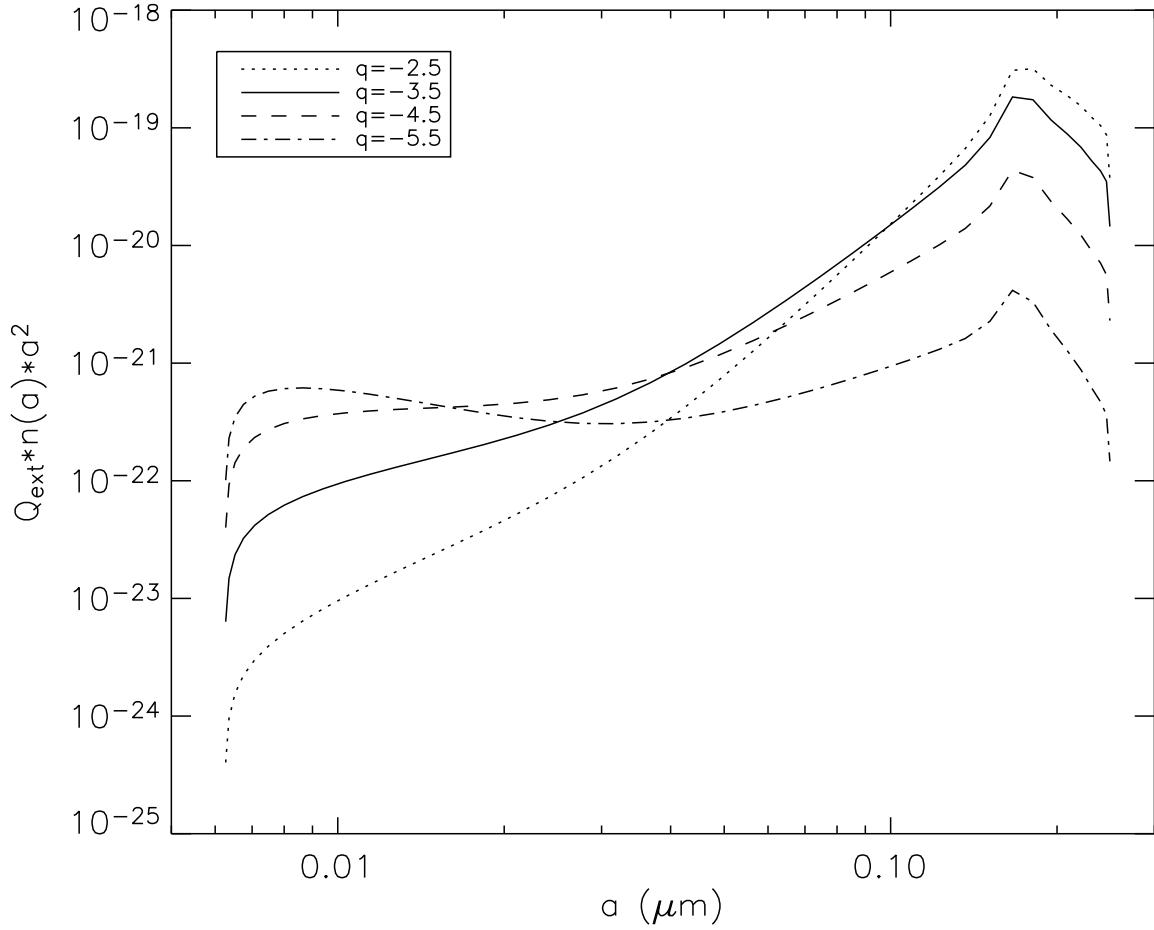


Fig. 2.— Plot of $Q(a)n(a)a^2$ from Eq. 3 for Al_2O_3 at a single wavelength ($1 \mu\text{m}$). The values shown for the power-law exponent are -2.5 (dotted), -3.5 (solid), -4.5 (dashed), and -5.5 (dash-dot).

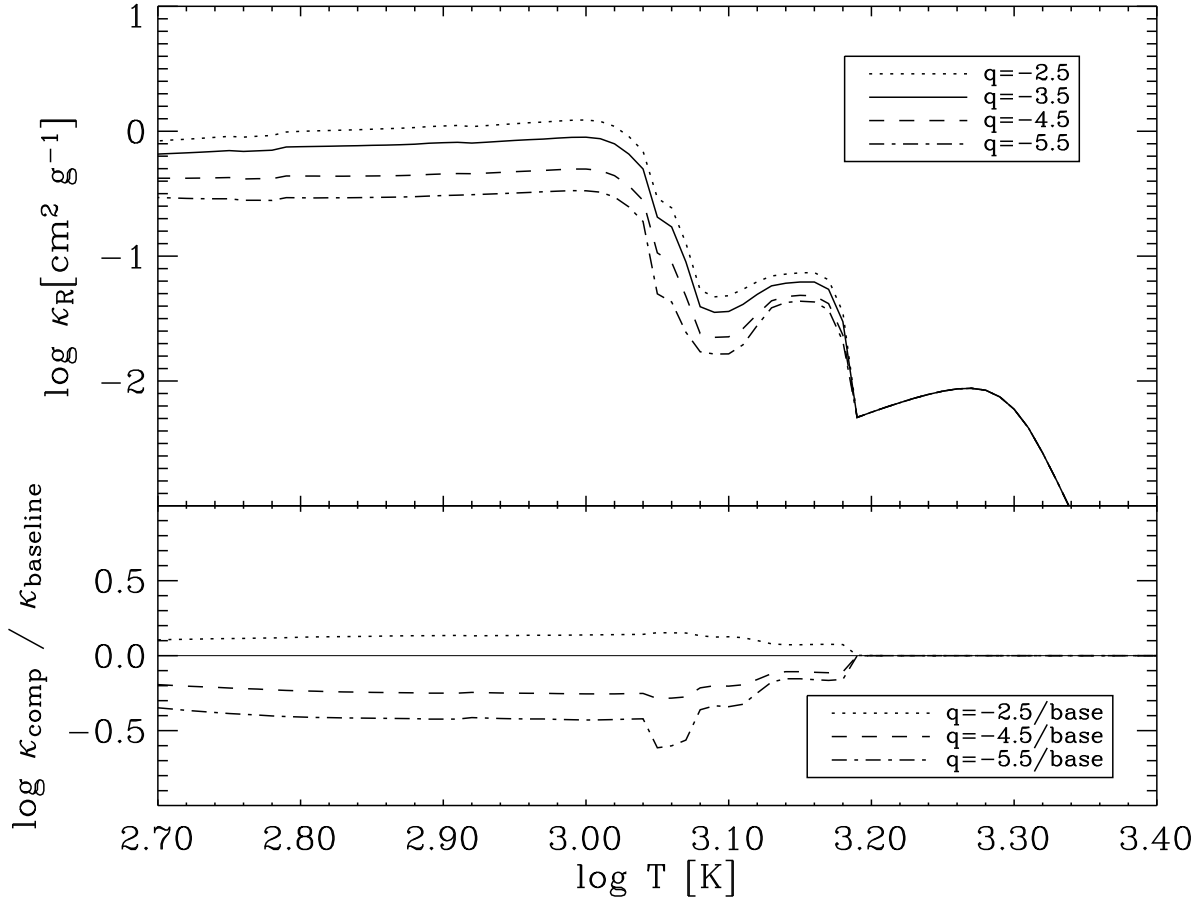


Fig. 3.— Comparison of opacities calculated with different values of the MRN power law exponent, q , describing the power law size distribution of grains. In the upper panel values of q are, from top to bottom, -2.5 (dotted), -3.5 (solid), -4.5 (dashed), and -5.5 (dash-dot). In the lower panel is the differences in the logarithm of the mean opacities for the various test cases and the baseline ($q = -3.5$) are shown. The dotted line is the logarithm of the ratio of the $q = -2.5$ case and the baseline, the dashed line is $q = -4.5$ case, and the dash-dot line represents the $q = -5.5$ case. The thin solid line is included to help guide the eye and is the value of the logarithm of one.

There are several features seen in the lower panel of Fig. 3 that deserve discussion such as the stair step behavior of the comparison with the $q = -5.5$ computation with the baseline. We include in our computations several species of grains in our total mean opacity with their different optical constants and extinction efficiencies. As different species appear or disappear from the EOS the mean opacity is affected in a variety of ways based upon the dominant species. More particularly, there is a large dip in the comparison with the $q = -5.5$ mean opacity between $3.04 \leq \log T \leq 3.08$. This feature, and the much smaller one seen in the $q = -4.5$ computation, is due to the differing effects on changing the size distribution for different species. In the lower panel of Fig. 3, at $\log T = 3.08$ the difference between the baseline and the $q = -5.5$ computation begins to move downwards as the Mg-silicates begin to dominate the opacity. The difference then moves upwards at $\log T = 3.04$ as solid Fe becomes the dominant source of opacity (see F05). Changing the size distribution in the same way for every species in our EOS has a different effect on that species’ contribution to the total mean opacity.

Notice also that the comparisons with the $q = -2.5$ and $q = -4.5$ are not symmetrical about the reference line 0.0. This shows that changing the value of the exponent does not lead to a linear, or clearly defined change in the mean opacity. This fact is not surprising by noting in Fig. 2 that the extinction efficiency, a function of grain size, rises with a , but not in a “linear” way.

It would be convenient to have a scaling factor to convert the baseline opacities to a set of mean opacities with a different grain size distribution and this may be possible away from transition zones. However, at those temperatures where the dominant grain species are changing a simple scaling factor is not possible.

2.2. Grain Size Distributions

The size distributions discussed in Section 1 have been added to our opacity code and to be complete we include a short summary of the KMH and WD grain size distributions. The size distribution from KMH is given by

$$n_i(a) = ka^q \exp(-a/a_b) \tag{5}$$

where a_b is the transition size for the exponential decay. The values chosen for our computations are discussed below.

A more sophisticated grain distribution, which includes a smoother transition from the

power-law to the exponential decay is given by WD for silicate dust and has the form

$$\frac{dn}{da} = \frac{k}{a} \left(\frac{a}{a_t} \right)^q F(a; \beta, a_t) \\ \times \begin{cases} 1, & 3.5 \text{ \AA} < a < a_t \\ \exp(-[(a - a_t)/a_c]^3), & a > a_t \end{cases}$$

where k is a normalization constant, q is the power-law exponent (originally α in WD), a_t and a_c provide for the cutoff and shape of the distribution, and the power-law exponent represented by q . The curvature of the function (changed by modifying β) is given by the term

$$F(a; \beta, a_t) \equiv \begin{cases} 1 + \beta a/a_t, & \beta \geq 0 \\ (1 - \beta a/a_t)^{-1}, & \beta < 0 \end{cases}$$

Similar distributions are assumed by WD for carbon or graphitic grains which include a log-normal distribution for the grain sizes to account for the very small grains thought emit the “Unidentified Infrared” (UIR) bands seen in the diffuse ISM. The comparisons in the present paper focus on oxygen-rich mixtures where carbon grains do not exist under these conditions.

For our comparisons we use the values given by WD for silicate dust in the ISM, that is $a_t=0.17 \mu m$ and $a_c=0.1 \mu m$ with a value of $\beta=0.3$ and a power-law exponent of -2.1 for all grain types. The computations using the KMH distribution use their stated parameters as well. That is, a_b is taken to be $0.14 \mu m$ and a value of -3.06 for q is used for silicate dust.

Figure 4 shows the comparison between Rosseland mean opacities computed with grain size distributions from MRN, WD and KMH. In the figure the mean opacities are shown in the upper panel and the differences in the logarithm of the opacities is shown in the lower panel. The results show that the mean opacities are somewhat similar, with MRN having the lowest values, WD having higher values, and KMH having the highest values of mean opacity. It is interesting to note that KMH, with a very simple exponential transition for large grains, tend to tail upwards at the lowest temperatures. At $\log T = 2.7$ (500 K), silicate grains are the dominant source of grain opacity, with solid iron grains falling in abundance in favor of FeS (see Fig. 1 of F05).

There is also a strange series of bumps in the lower panel of Fig. 4 at intermediate temperatures, $3.00 < \log T < 3.15$. As discussed in the previous section, these temperatures are a transition region where the strongest opacity source is passing from minor grain species to the silicates to solid Fe. Different grain species have different contributions to the opacity

based upon which form of the size distribution is used due to different optical constants and extinction efficiencies. The feature seen in the lower panel of Fig. 4, centered at $\log T = 3.08$, in the computations with KMH compared with the baseline is much more pronounced than the computations with WD. The difference between the KMH and WD grain distributions is how the size transition to large grains is treated. The minor grain species are much more sensitive to the KMH distribution than the solid Fe grains are, since when solid Fe dominates the opacity both the KMH and WD computations appear to be a simple scaling factor greater in the mean opacity.

As discussed in the previous section, there does appear to be a simple scaling factor that might apply to the grain distributions, but only for a limited range in temperature, $2.80 \leq \log T \leq 3.02$. At other temperatures, where the strongest opacity source is changing from one grain species to another, no such simple scaling factor is evident.

Overall the effect on the mean opacity is fairly significant with the KMH calculation differing from the baseline (MRN) by 0.27 dex at $\log T = 2.9$ (800 K), or nearly a factor of 3. As Fig. 4 shows the difference from the baseline is not constant with temperature, especially in the regions where the significant contributors to the opacity are from different grain species (with different extinction efficiencies). For example around $\log T \sim 3.15$ the differences between the computations are smaller than at cooler temperatures. This implies that arbitrarily adding a factor of 3 to the mean opacity tables of F05 to mimic the effects of different size distributions is not a good approximation. This is particularly true when combined with the mean opacity changes with differing size distribution exponents as described above.

2.3. Grain Porosity

Calculations of grain efficiencies due to grain porosity are taken from Bohren & Huffman (1983). To initially probe the effect of porosity on the mean opacity we assume that the vacuum inclusions are spherical and we use either the Maxwell-Garnett or the Bruggeman average dielectric constant for the grain/vacuum composite. Maxwell-Garnett is more appropriate for a mixture where the matrix and inclusions are well defined. The Bruggeman approximation is more symmetric and valid for a two-component mixture with matrix and inclusions indistinguishable. As Bohren & Huffman (1983) discuss both Maxwell-Garnett and Bruggeman are equally valid, but either one or the other will be more valid in a particular circumstance.

In our computations we find that certain grain species misbehave when using the Brugge-

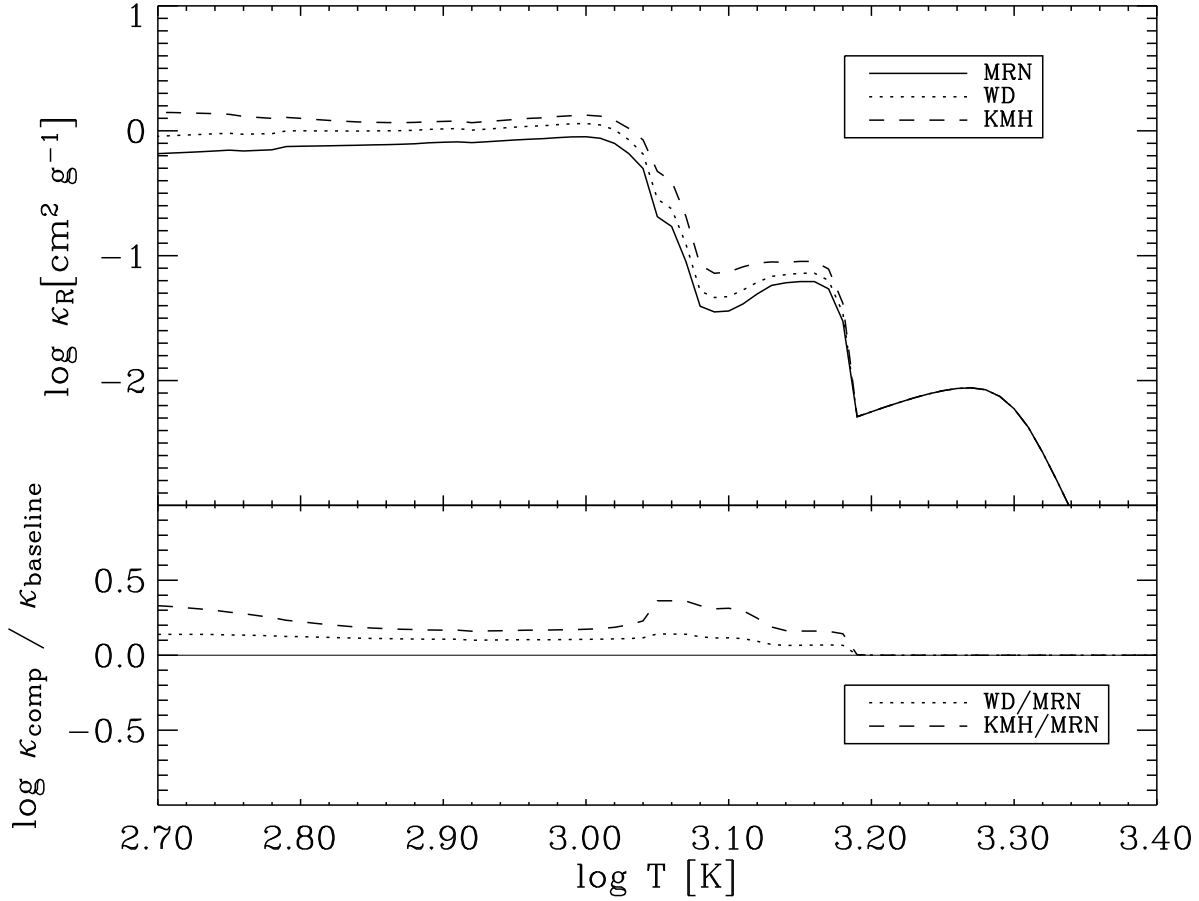


Fig. 4.— Comparison of the mean opacity due to differing grain size distribution models. In the upper panel, the solid line is the mean opacity when using the MRN distribution, WD is represented by the dotted line, and the model of KMH is shown by the dashed line. In the lower panel the differences are shown as in Fig. 3, with the thin solid line at the 0.0 axis shows no change to the opacity, the dotted line compares WD with the baseline, and the dashed line compares KMH with the baseline. See the text for detailed discussion.

man approximation. Most particularly troubling is solid Fe. At certain wavelengths the k portion of the optical constant will be unphysically negative, causing the mean opacity to increase discontinuously by large factors. To test our method we have utilized the publicly available average dielectric routines of Ossenkopf (1991) and found that program fails to compute porous Fe grains without either blowing up with a fatal error, or producing negative parts of the optical constants. We have decided to remove Fe from the porosity computation and let it remain solid and not porous. We assume that the other grain species are valid under the Bruggeman assumption, the EOS is mostly dominated by MgSiO_3 and Mg_2SiO_4 at 1000 K and below (see F05, Fig. 1).

Results for a range of grain porosities, denoted by the volume fraction f , are shown in Figure 5 with the mean opacities shown in the upper panel. The baseline value is $f=0.0$ (solid grains) and the tested values include $f = 0.1, 0.25, 0.5,$ and 0.8 . Recent work by Chiar & Tielens (2006) report porosities of grains in the ISM as being between 25% and 50% vacuum by volume, in line with previous studies by Wolff et al. (1993). The lower panel shows the opacity differences compared with the baseline of $f = 0$.

As the porosity of grains is increased, the the total mean opacity is mostly unaffected, except for the largest f value. This is somewhat intuitive in that the mean opacity is already dominated by small particles, making those small particles slightly larger, does not change the mean opacity greatly. At the largest value of porosity, $f = 0.8$ the mean opacity does change by as much as 50% at the lowest temperature shown. Note at “intermediate” temperatures, $3.05 < \log T < 3.13$, the lower panel of Fig. 5 clearly shows that the mean opacity decreases with increasing porosity. The materials responsible for most of the mean opacity at these temperatures are SiO_2 , calcium-silicates, and MgAl_2O_4 for the most part (see F05, Fig. 1). As these types of grains become larger and more porous that they also become more transparent, unlike the silicates at cooler temperatures, where the mean opacity slightly increases with porosity.

2.4. Aggregate Grains

To explore the use of aggregate grains and their effects on the Rosseland mean opacity we compute the average dielectric function as outlined by Bohren & Huffman (1983) using effective medium theory (EMT). More specifically we assume Maxwell-Garnett theory for aggregates which is valid as long as the inclusions obey the Rayleigh limit as illustrated by Wolff et al. (1998). We use this simple EMT approximation rather than a more formal solution such as a discrete-dipole approximation (DDA) due to limits on computational time. In addition, many of the features of a DDA are not needed for mean opacities computations,

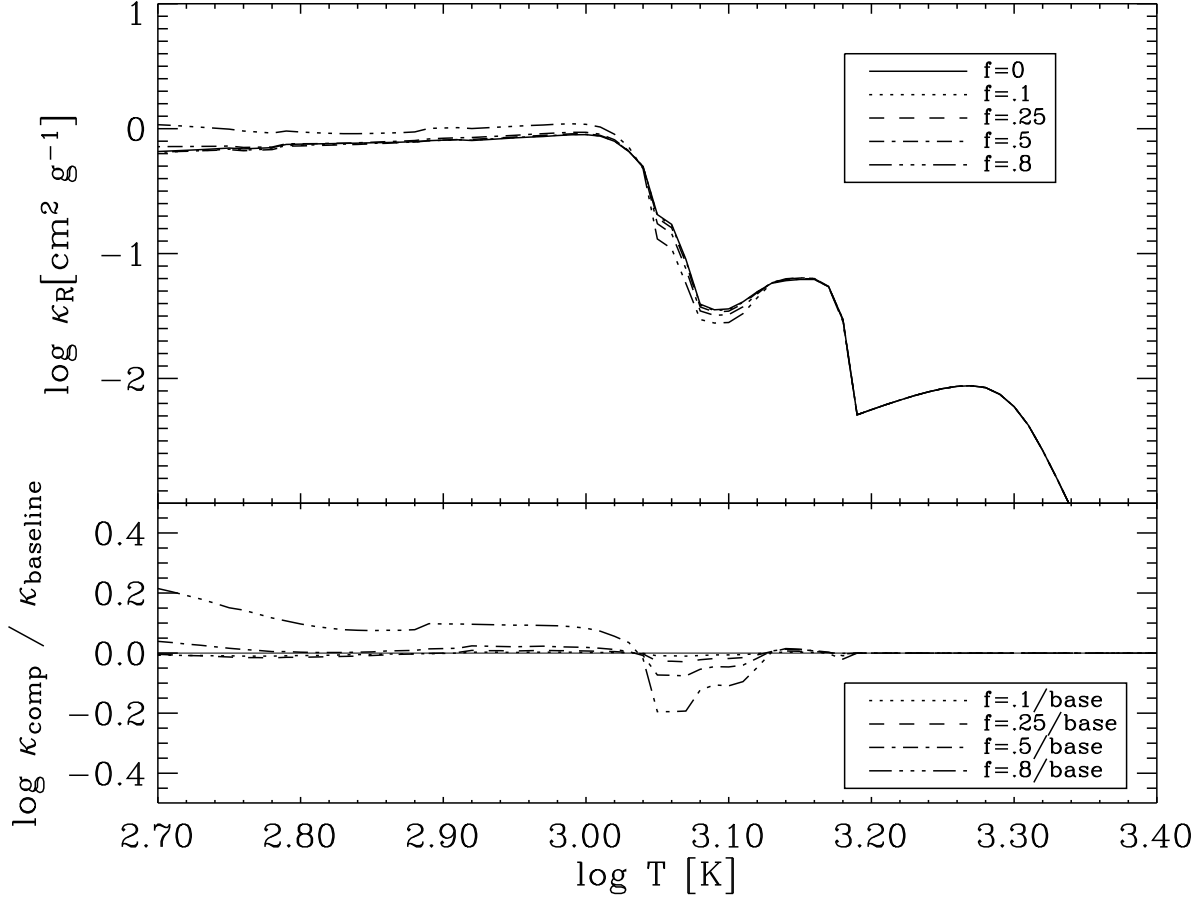


Fig. 5.— Comparison of varying the porosity of grains. In the upper panel, the mean opacities are shown. The baseline calculation is the solid line with dust porosity, $f=0.0$, the dotted line is $f=0.1$, the dashed line is $f=0.35$, the dash-dot line is $f=0.5$, and the dash-dot-dot line is $f=0.8$. In the lower panel the differences are shown as in Fig. 3, with the porosity $f=0.1$ compared with the baseline as dotted, $f=0.25$ as dashed, $f=0.5$ as dash-dot, and $f=0.8$ as the dash-dot-dot line.

such as the scattering and polarizaton phase functions.

To compare with the baseline runs as outlined above we assume an aggregate grain that is similar in composition to the silicate species computed in our EOS at $\log T = 2.9$ (800 K) and with ratios similar to silicates found in the inclusions of a typical meteorite such as Semarkona as discussed in Hewins et al. (1996). While our EOS did not identically produce the Semarkona results, qualitatively it was fairly close; we compared our EOS with Semarkona and choose a median value. The ratios of enstatite, forsterite, fayalite, and silicon dioxide were assumed to be 42%, 36%, 12%, and 10% respectively. We computed the average dielectric functions using the routines of Ossenkopf (1991) with the stated ratios. Solid iron grains were kept separate from the aggregate as is found in meteoritic inclusions. The mean opacity was then computed at a single temperature and density ($\log R$) point and compared with the baseline. Repeating this numerical experiment at lower temperatures did not dramatically change the results

The comparisons show that aggregate grains have a lower mean opacity, on the order of 0.05 dex (12%) below the baseline, which is a smaller change shown in Fig. 3 for changes in the grain size exponent q from -3.5 to -4.5. The amount of change in the mean opacity for aggregate grains from the baseline is very modest and near the estimated range of error in the grain thermodynamic and optical data of 0.02 dex (5%) based upon comparisons with other opacity databases (see F05). This result implies that including or not including aggregate grains in the computation of the mean opacity is not an important decision when computing mean opacity tables.

2.5. Grain-to-Gas Ratio

The opacities of F05 were not intended to be used in non-equilibrium conditions. However, we can mimic such environments such as conditions of gravitational “rain-out”. If the gas/dust environment is under a gravitational influence with insignificant radiation pressure, then grains that should appear in the equaton of state will settle down into the gravitational potential and “disappear” from view. This will leave behind the apperance of a grain depleted, or a gas rich, environment. This is best simulated by letting the grains appear in the equation of state, but not counting their opacities. Figure 6 shows such simulations. The baseline amount from F05 includes 100% of the grain opacity for each species. The upper panel of Fig 6. shows the effects of including 50%, 10% and 1% of the total grain opacity.

The effect on the mean opacity is roughly equivalent to the amount of grains removed from the grain opacity term. That is, if the grain opacity is cut in half, then the total mean

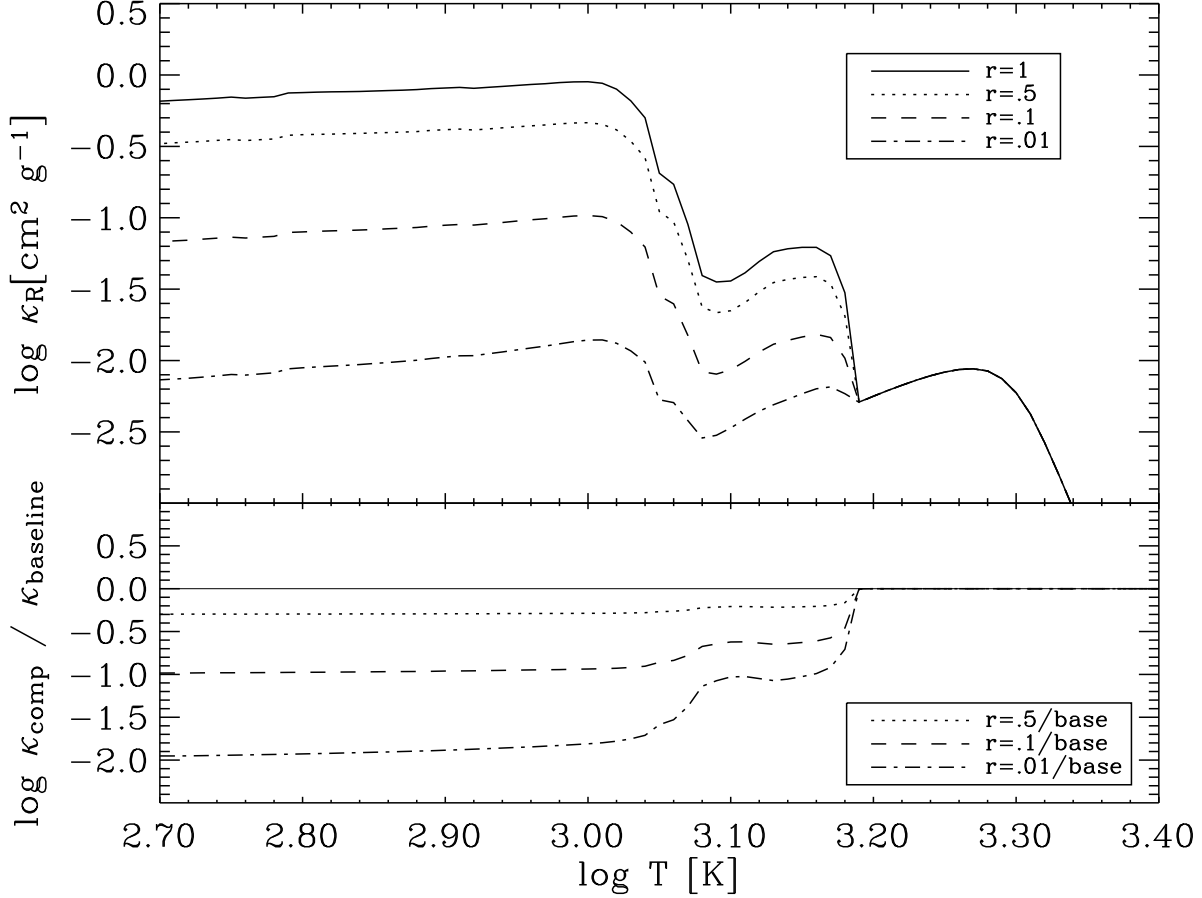


Fig. 6.— Comparisons of total Rosseland mean opacity with varying amounts of grain opacity included. In the upper panel, the solid line is the baseline calculation (100% of the grain opacity included), the dotted line includes only 50%, the dashed line 10% and the dash-dot line only includes 1% of the grain portion of the opacity. In the lower panel the differences with the baseline are shown as in Fig. 3 with the dotted line comparing the 50% ratio to the baseline, the dashed line comparing the 10% ratio, and the dash-dot line the 1% ratio.

opacity is also roughly half of the baseline value because the grain opacity usually completely dominates the total opacity whenever grains are present. This is easy to see in the lower panel of Fig. 6. Note that this effect is not true for all temperatures however. At higher temperatures, the differences in the opacities (between the baseline and the test cases) are not smooth. Just below the grain appearance temperature at $\log T \sim 3.2$ there is still a modest molecular opacity present. If a small amount of grain opacity, say 1%, is added to the (now) larger molecular opacity, the roughly linear scaling does not apply. As the molecular opacity drops at lower temperature, there is a roughly linear relationship between the amount of dust included in the monochromatic opacity and the total mean opacity. This result means that to a reasonable approximation the opacity tables of F05 could, in principle, be modified to account for the effect of a grainless gas by multiplying by the desired factor, but only at the coolest temperatures. It would not be advisable near the transitions between molecules and grains dominating the opacity.

3. Discussion

This work implies that caution should be taken when requesting or downloading prefabricated opacity tables and using them in environments where grain condensation is significant. It is important to include the physical effects that are desired to have accurate opacities, most notably changes in the size distribution can greatly affect the Rosseland mean.

Opacity tables for the F05 base set are available for download at our web site at <http://webs.wichita.edu/physics/opacity>. Custom opacity tables for non-standard compositions or for different physical assumptions are available upon request, as are tables in gas density or gas pressure space instead of $\log R$. Note that a full set of opacity tables as outlined in Ferguson et al. (2005) with (now) 155 values of hydrogen, X, and metal, Z, abundances take approximately a week of computer time, due to our full treatment of the molecular opacity sampling.

We acknowledge the anonymous referee for the suggested references and other comments that have improved this paper. Low temperature astrophysics at Wichita State University is supported by NSF grant AST-0239590, NASA LTSA grant NAG5-3435 with matching support from the State of Kansas. We also acknowledge the support from the National Science Foundation under Grant No. EIA-0216178 and Grant No. EPS-0236913, matching support from the State of Kansas and the Wichita State University High Performance Computing Center.

REFERENCES

- Bohren, C. F. & Huffman, D. R. 1983, *Absorption and scattering of light by small particles* (New York: Wiley, 1983)
- Chiar, J. E. & Tielens, A. G. G. M. 2006, *ApJ*, 637, 774
- Clayton, G. C., Wolff, M. J., Sofia, U. J., Gordon, K. D., & Misselt, K. A. 2003, *ApJ*, 588, 871
- Draine, B. T. & Li, A. 2001, *ApJ*, 551, 807
- Ferguson, J. W., Alexander, D. R., Allard, F., Barman, T., Bodnarik, J. G., Hauschildt, P. H., Heffner-Wong, A., & Tamanai, A. 2005, *ApJ*, 623, 585
- Grevesse, N. & Noels, A. 1993, *Origin and Evolution of the Elements*
- Hewins, R., Jones, R., & Scott, E. 1996, *Chondrules and the Protoplanetary Disk* (Chondrules and the Protoplanetary Disk, Edited by Roger Hewins and Rhian Jones and Ed Scott, pp. 360. ISBN 0521552885. Cambridge, UK: Cambridge University Press, June 1996.)
- Iglesias, C. A. & Rogers, F. J. 1991, *ApJ*, 371, 408
- . 1993, *ApJ*, 412, 752
- . 1996, *ApJ*, 464, 943
- Kim, S.-H., Martin, P. G., & Hendry, P. D. 1994, *ApJ*, 422, 164
- Li, A. & Draine, B. T. 2001, *ApJ*, 554, 778
- Mathis, J. S. 1996, *ApJ*, 472, 643
- Mathis, J. S., Rumpl, W., & Nordsieck, K. H. 1977, *ApJ*, 217, 425
- Mathis, J. S. & Whiffen, G. 1989, *ApJ*, 341, 808
- Ossenkopf, V. 1991, *A&A*, 251, 210
- Rogers, F. J. & Iglesias, C. A. 1992a, *ApJS*, 79, 507
- . 1992b, *ApJ*, 401, 361
- Rogers, F. J., Swenson, F. J., & Iglesias, C. A. 1996, *ApJ*, 456, 902

- Seaton, M. J., Yan, Y., Mihalas, D., & Pradhan, A. K. 1994, MNRAS, 266, 805
- Voshchinnikov, N. V., Il'in, V. B., & Henning, T. 2005, A&A, 429, 371
- Weingartner, J. C. & Draine, B. T. 2001, ApJ, 548, 296
- Wolff, M. J., Clayton, G. C., & Gibson, S. J. 1998, ApJ, 503, 815
- Wolff, M. J., Clayton, G. C., Martin, P. G., & Schulte-Ladbeck, R. E. 1994, ApJ, 423, 412
- Wolff, M. J., Clayton, G. C., & Meade, M. R. 1993, ApJ, 403, 722